HTML ABSTRACT + LINKS

Combinatorial and high-throughput measurements of the modulus of thin polymer films

Christopher M. Stafford,[a] Shu Guo, Christopher Harrison,[b] and Martin Y. M. Chiang
Polymers Division, National Institute of Standards and Technology, Gaithersburg, Maryland 20899

(Received 15 November 2004; accepted 30 January 2005; published online 18 May 2005)

We describe the design and refinement of a high-throughput buckling-based metrology for ascertaining the mechanical properties (e.g., modulus) of combinatorial thin polymer film libraries. We provide critical details for the construction of a suitable strain stage, describe sample preparation, and highlight methods for high-throughput data acquisition and data analysis. To illustrate the combinatorial and high-throughput capability of this metrology, we prepare and evaluate films possessing a gradient in the elastic modulus and compare the results with an analytical expression derived from composite beam theory. Application of this metrology is very simple and practically any laboratory, academic or industrial, can perform such measurements with only modest investment in equipment. Although developed as a platform for investigating combinatorial libraries, researchers can take advantage of the high-throughput nature of this metrology to measure noncombinatorial film specimens as well. [DOI: 10.1063/1.1906085]

I. INTRODUCTION

Considerable attention has been devoted to developing fabrication strategies for constructing combinatorial material libraries as well as tools for characterizing the chemical properties of such libraries. Less attention has been dedicated to designing high-throughput metrologies for probing the physical or engineering properties of combinatorial libraries. For example, thin polymer films are critical to technological applications such as advanced optics, microelectronics, data storage, and bioengineering.[1] The mechanical properties and stability of such ultra-thin (submicrometer) films are paramount to the fabrication, performance, and reliability of devices. For instance, the semiconductor industry uses lithography to pattern nanostructures in polymeric resists, followed by developing and rinsing steps with aqueous solutions to remove unreacted material from in between the nanostructures. These nanostructures, which can be viewed as free-standing thin films with widths of 100 nm down to 10 nm, often collapse during drying due to the large Laplace pressures generated by a liquid meniscus between the walls of the nanostructures.[2–4] The design and incorporation of higher modulus materials into the lithography process can improve resistance to collapse and thus circumvent this fabrication issue. In this paper we present a high-throughput metrology that allows researchers to rapidly measure the elastic modulus for hundreds of points across a combinatorial library in a matter of minutes.

Several techniques have emerged to measure the mechanical properties of both supported and unsupported polymer thin films, the most prominent being instrumented indentation methods that have been scaled down to the micro- and nano-indentation regime.[5–7] Here, a point load is applied to a supported thin film and the load/penetration depth curve is recorded over a complete loading/unloading cycle. From this load/displacement data, the modulus of the thin film can be calculated, although these techniques tend to overestimate the modulus of the film due to contributions and interactions with the underlying substrate. In addition to instrumented indentation, there are surface acoustic/guided wave methods for probing the near-surface mechanical properties of polymer thin films, the primary examples being Brillouin light scattering[8,9] and surface acoustic wave spectroscopy.[10] Finally, bulge tests[11–14] are capable of measuring modulus and residual stress of thin films, but require free standing, or at least partly free standing, films. The membrane is pressurized from one side and the deflection at the center is recorded as function of applied pressure. The pressure-displacement relationship is given using plate theory and finite element analysis, and Young's modulus can be determined through fitting the experimental data with analytical or numerical solutions. Unfortunately, many of these techniques are not positioned to be applied as high-throughput measurement platforms for submicron polymer films.

Recently we reported on a new buckling-based metrology[15] that is able to measure the elastic modulus of polymer films mounted on a relatively thick, soft substrate. In this paper, we detail the design and application of this metrology with emphasis on sample preparation, apparatus design, data collection, and image analysis. We demonstrate the combinatorial and high-throughput capacity of this technique with a one-dimensional modulus gradient fabricated by laminating two layers of materials with disparate moduli.

II. REVIEW OF RELEVANT BUCKLING MECHANICS

Many researchers have studied the instability of a beam or plate supported by an elastic foundation.[16–20] Buckling can occur when a compressive stress is applied to a substrate/film laminate. In an effort to minimize the total elastic strain

[a]Author to whom correspondence should be addressed; electronic mail: chris.stafford@nist.gov
[b]Present address: Sensor Physics Department, Schlumberger-Doll Research, Ridgefield, Connecticut 06877.

Downloaded 24 May 2005 to 129.6.154.144. Redistribution subject to AIP license or copyright, see http://rsi.aip.org/rsi/copyright.jsp

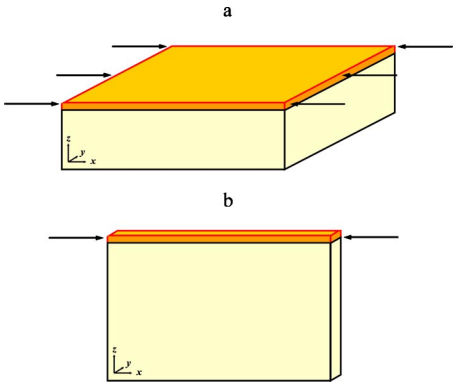

FIG. 1. (Color online) Schematics showing (a) plane strain and (b) plane stress conditions for a thin film laminated onto an infinitely thick substrate.

energy of the system, the laminate will have a propensity to buckle if the applied compressive stress/strain exceeds a critical value. The critical stress, σ_c, needed to buckle the laminate is dependent on the material properties of the substrate and film, as shown in the following equations:[19]

$$\sigma_c = \sqrt[3]{\frac{9}{64}\frac{E_s^2 E_f}{(1-\nu_s^2)^2(1-\nu_f^2)}}, \tag{1}$$

where E is Young's modulus, and ν is Poisson's ratio. Subscripts f and s correspond to the film and substrate, respectively. The wavelength of the buckling instability is given by

$$\lambda = 2\pi h\left[\frac{1-\nu_s^2}{3(1-\nu_f^2)}\frac{E_f}{E_s}\right]^{1/3}, \tag{2}$$

where h is the thickness of the upper film. Equation (2) can be rearranged to elucidate the dependence of the upper film modulus on the wavelength of the buckles as well as the material properties of both the film and substrate:

$$E_f = \left(\frac{\lambda}{2\pi h}\right)^3\left[\frac{3(1-\nu_f^2)}{1-\nu_s^2}E_s\right]. \tag{3}$$

Therefore, by knowing the material properties of the substrate and wavelength of the buckled film and film thickness, the film's Young's modulus can be calculated. The above equations are derived for a plate geometry, in which the film's width is large compared to its thickness. An alternate solution has been reported for a beam model,[16] in which the width of film and substrate are small compared with their length, but comparable to the film's thickness. Figure 1 illustrates these two geometries. Most thin films exhibit characteristics of plates, as shown in Fig. 1(a), because the film thickness is normally small compared to the other two dimensions. However, in some situations, a beam model shown in Fig. 1(b) could be applicable, e.g., a fine thin line fabricated by microlithography patterning or direct write methods.[21] In the following sections, we will outline how we employ this phenomenon to probe the mechanical properties of polymer thin films having gradients in material properties.

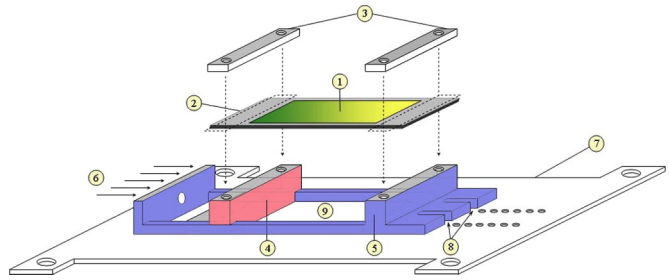

FIG. 2. (Color online) Strain stage design: ① gradient film specimen, ② PDMS substrate, ③ clamps, ④ stationary grip, ⑤ sled grip, ⑥ motorized actuator for controlling displacement, ⑦ mounting plate, ⑧ grooves for locking in strain, and ⑨ window for conducting transmission experiments.

III. EXPERIMENTAL SETUP AND OPERATION

A. Design of strain stage

We designed and constructed a custom strain stage for conducting our buckling-based metrology. The geometry and dimensions of the stage were chosen such that the stage can be mounted onto a number of imaging platforms in our laboratories, including an optical microscope, a small angle light scattering (SALS) apparatus, and an atomic force microscope (AFM). Each of these imaging platforms can be automated to varying degrees to provide a measure of the buckling wavelength either in real space or Fourier space.

The strain stage was designed based on a slide-type construction as illustrated in Fig. 2. The gradient film (1) is transferred to a 75×25 mm^2 strip of silicone (2), which is subsequently mounted and clamped (3) to the strain stage. The first "grip" (4) of the stage is held stationary while the sled/second "grip" (5) is free to move. Strain is applied by the use of a motorized actuator (6) attached to one end of the sled. Both the strain stage and actuator assemblies are mounted to individual aluminum plates (7), which are also mounted to a solid aluminum support. On the opposite end of the sled are grooves (8) for locking the sled down, which allow the degree of strain to be fixed or maintained. When this is done, the strain stage can be disengaged from the motorized actuator assembly and removed from the support block, at which time the entire strain stage can be transported easily between imaging platforms for ascertaining the buckling wavelength and, when desired, the buckling amplitude. A window (9) was machined into both the aluminum plate and support directly under the suspended specimen to allow for passing a laser directly through the sample. The entire assembly has a black anodized finish to minimize light reflections. An image of the strain stage assembly is shown in Fig. 3.

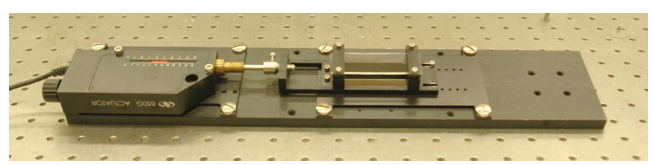

FIG. 3. (Color online) Image of our custom-designed strain stage for conducting buckling measurements.

Downloaded 24 May 2005 to 129.6.154.144. Redistribution subject to AIP license or copyright, see http://rsi.aip.org/rsi/copyright.jsp

B. Sample preparation

Poly(dimethylsiloxane) (PDMS, Sylgard 184, Dow Chemical)[22] was chosen as the elastic foundation since it is optically transparent, it approximates an ideal elastomer, and its modulus can be tuned by the mixing ratio of base to curing agent. Typically, a 10:1 ratio of base to curing agent is used in our studies. The PDMS mixture is degassed over 30 min under vacuum before spreading onto an 8×8 in^2 sheet of plate glass. The volume of PDMS prepolymer prepared is carefully chosen to result in a final thickness of 1 to 2 mm. If the mixture is immediately cured at elevated temperature, the thickness of cured PDMS would be nonuniform and the surface would not be smooth. Therefore, the mixture is allowed to flow, level, and partially cure for 12 h at room temperature, and then fully cured in a forced air oven at 70 °C for 1.5 to 2 h. The resulting PDMS sheet is then cut into individual pieces with dimensions of 25×75 mm^2 using a manual punch. One PDMS section was reserved for measuring the Young's modulus of the substrate material. Typical Young's moduli of the PDMS ranged from 1.5 to 2.0 MPa, as measured on a Texture Analyzer (Model TA.XT2i, Texture Technologies Corp.).

For preparation of the polymer film to be measured, a dilute solution of polymer is typically flow coated or spin cast onto a polished silicon wafer. Just prior to coating, the surface of the silicon wafer is rendered hydrophilic by exposure to UV/ozone for 30 min. Similar results can be obtained by cleaning with oxygen plasma. Spin coating yields films with exceptionally uniform thickness that can be measured using spot interferometry or ellipsometry. Multiple measurements across the sample can be made and the average thickness and standard deviation can be calculated. Flow coating affords preparation of films possessing a gradient in thickness, but a complete thickness map[15] must be acquired of the gradient film, and this map must be precisely correlated to the specific positions where the buckling wavelength is to be measured. We find that this is easily achieved by automated interferometry thickness measurements across an *x*-*y* grid of points and the use of fiduciary marks, respectively.

Films are transferred from the silicon wafer to PDMS substrates by aqueous immersion. In most cases, the PDMS is elongated and held fixed in the strain stage prior to film transfer, such that release of the applied strain results in an application of a net compressive strain on the film. The film on silicon is then placed face down on the PDMS substrate. Visual observation indicates the PDMS wets and softly adheres to the surface of the polymer film. Immersion of the multilayer stack in water results in the transfer of the polymer film to the PDMS due to the wicking of water into the polymer/silicon interface. The entire stage assembly is then removed from the water and gently dried using compressed nitrogen. Buckling of the film/substrate occurs upon compression, observable by the iridescent color of the buckled region, as can be seen in Fig. 4. Ideally, the entire film would buckle simultaneously, but imperfections in the film and substrate as well as distortions in the strain field can cause portions of the film to buckle before others. Thus, the degree of compression is manually adjusted via the actuator until the entire film is buckled, at which time the measurement of wavelength is performed and the compressive strain recorded.

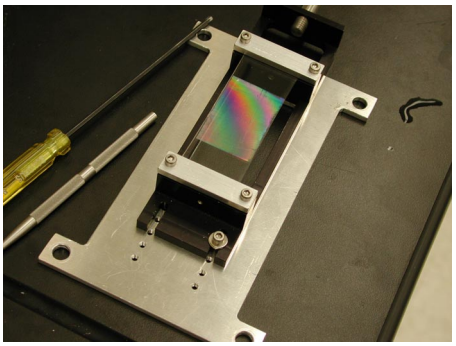

FIG. 4. (Color online) Image of just the sled component of the strain stage. A specimen has been loaded onto the strain stage and subsequently buckled, as evidenced by the iridescent color resulting from micron-sized wrinkles on the surface of the laminate. This image also demonstrates that the applied strain can be locked in by using the grooves in the sled and the array of threaded holes in the mounting plate.

C. Data collection

After preparation and mounting of samples onto the strain stage, the buckling instability is initiated by application of strain. The magnitude of stress necessary to trigger the instability is a function of both the moduli and Poisson's ratios of the film and substrate [see Eq. (1)]. This buckling introduces highly periodic wrinkles where the associated buckles are oriented perpendicular to the direction of strain. The wrinkling wavelength can be measured in a variety of ways, including both contact and noncontact methods.

Noncontact methods include two primary methodologies: optical microscopy and SALS. Optical microscopy provides the most direct method to verify the uniformity of the buckles, but it also requires focusing, an aspect which can add an additional complication and time-consuming step when implementing an automated high-throughput measurement. Auto-focus modules often do not live up to their promise and, furthermore, can add a rate-limiting step for the hundreds or even thousands of measurements associated with routine high-throughput screening. Moreover, it can be difficult to unambiguously ascertain the actual wrinkling period as buckle crests and troughs occasionally, but not always, can be difficult to discern. However, for samples that are opaque or of wavelengths much greater than 50 μm, this can be the only route. Images can be collected with a conventional charged coupled device (CCD) camera or digital camera mounted on the microscope. For high-throughput work, automation of stage motion, image focusing, and image acquisition is readily available. However, for all such work, long-working distance objectives are recommended such that the microscope objective does impede motion of the strain stage. Calibration of microscope images is carried out by obtaining images of a stage micrometer or other standards with well-measured dimensions. Image analysis for data collected on the optical microscope is discussed in the next section.

In contrast to microscopy, SALS provides a particularly fast and convenient method for high-throughput data acqui-

Downloaded 24 May 2005 to 129.6.154.144. Redistribution subject to AIP license or copyright, see http://rsi.aip.org/rsi/copyright.jsp

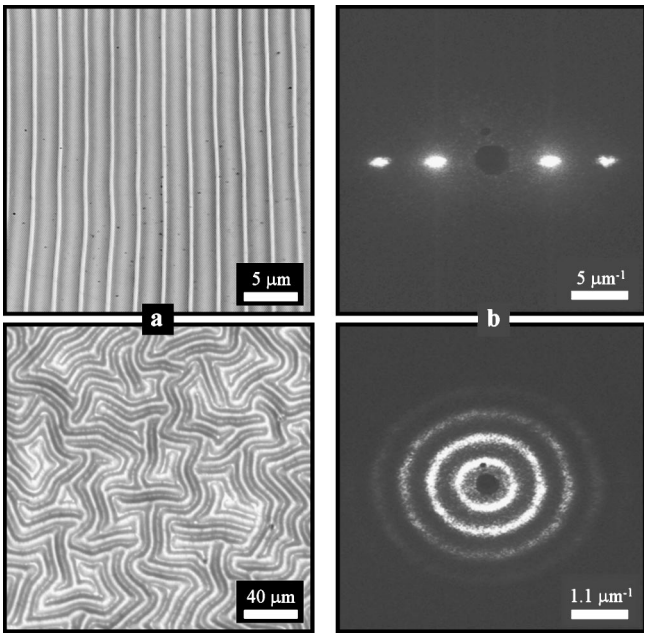

FIG. 5. Examples of (a) optical microscope images and (b) resulting SALS patterns of anisotropic (top) and isotropic (bottom) buckling patterns.

sition and analysis, and is enabled by the optical transparency of the PDMS substrate. Conventional SALS apparatuses with rudimentary automation are becoming more affordable due to advances in lasers, CCD cameras, and computerized translation stages. No optical lenses are necessary and a sheet of paper works nicely as a diffuser/imaging screen. We find that a conventional 8-bit (256 levels) grayscale camera provides sufficient sensitivity for our purposes. Calibration of the scattering wave number in one dimension versus image pixel number can be carried out with a diffraction grating, such as a Ronchi ruling. We find that a third-order polynomial fit typically suffices to make a one-to-one correspondence between pixel and wave number q. After calibration, identification of the diffraction peaks is straightforward and can be further refined by application of a scattering function, such as a Gaussian. Our SALS apparatus is outfitted with an automated x-y translation stage to facilitate mapping of the buckling wavelength as a function of spatial position on the sample.

While the two methods mentioned above measure the lateral length scale of the buckles, they do not provide topographical information such as buckling amplitude.[23] One direct method to obtain full three-dimensional topographical information is profilometry, such as provided by AFM. However, this technique is sufficiently time consuming that it would be all but impractical for high-throughput work. Analysis of AFM images will be discussed below.

D. Image and data analysis

To best quantify the wavelength of the resulting buckling patterns, we choose to conduct all image analyses in Fourier space. This approach yields the dominant wave vector, q_m (μm^{-1}), present in the system. The dominant wave vector can then be converted to wavelength using the relationship

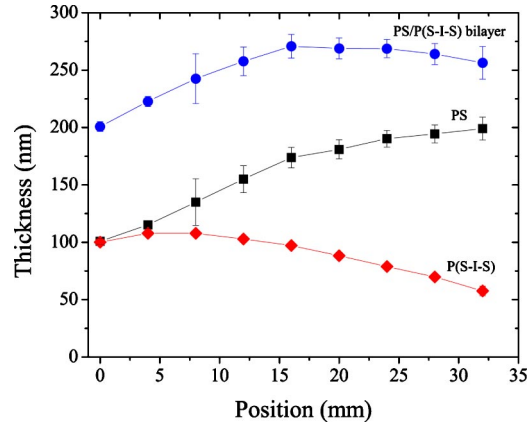

FIG. 6. (Color online) Thickness profile of PS, P(S-I-S), and the laminated bi-layer. The error bars represent one standard deviation of the data, which is taken as the experimental uncertainty of the measurement. Some error bars are smaller than the symbols.

$$\lambda_m = 2\pi/q_m, \tag{4}$$

where λ_m (μm) is the dominant wavelength of the buckling instability. If images of the buckling pattern are collected using an optical microscope, the real-space images must first be converted to Fourier space using fast Fourier transform (FFT) algorithms provided in many commercial packages including MatLab, IDL, and Image Pro. SALS images are by definition already in Fourier space, so no further transforms are needed. If the buckling pattern is isotropic, the resulting FFT will be a series of concentric circles; if the buckles are aligned, the resulting FFT will be a series of peaks (see Fig. 5). In the former case (isotropic), the dominant wave vector can then be ascertained by taking an azimuthal average of the intensity (I) as a function of q. In the latter case (aligned), however, this process can be simplified by performing a line scan through the center of the peaks. The resulting $I(q)$ plot is smoothed using an adjacent averaging method; typically, a seven-point smoothing function is used. Finally, an automated routine is used to determine the q-position of maximum intensity (q_m) for first- and (when possible) second-order peaks ($2q_m$, ideally). This value of q_m is then converted to λ_m through Eq. (4), which is used to calculate the film modulus through Eq. (3). If the specimen only contains a gradient along one axis, multiple images can be collected along the nongradient axis (uniform material properties) to generate the error or uncertainty of the measurement.

IV. EXAMPLE: MODULUS GRADIENT

To demonstrate the viability of this buckling-based metrology as a combinatorial and high-throughput technique, we generate a modulus gradient consisting of a bi-layer of polystyrene-polyisoprene-polystyrene [P(S-I-S)] triblock copolymer (Vector 4411, Dexco Polymers LP) and polystyrene (PS) films. Dissolved P(S-I-S) and PS solutions were separately flow-coated onto a silicon wafer to form films with gradients in film thickness. By placing the P(S-I-S) film on top of the PS film with the thickness gradients parallel to one another, a modulus gradient was formed in the P(S-I-S)-PS

Downloaded 24 May 2005 to 129.6.154.144. Redistribution subject to AIP license or copyright, see http://rsi.aip.org/rsi/copyright.jsp

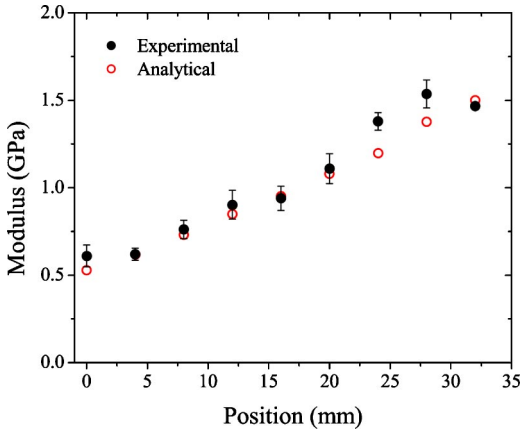

FIG. 7. (Color online) Modulus as a function of position in the laminated PS/P(S-I-S) bi-layer for both experimental data (closed circles) and the analytical solution (open circles). The error bars represent one standard deviation of the data, which is taken as the experimental uncertainty of the measurement. Some error bars are smaller than the symbols.

bi-layer along the flow-coating direction. Using composite beam theory, the resultant effective modulus, E_{eff}, of a bi-layer can be calculated as follows:

$$E_{\text{eff}} = \frac{1 + m^2 n^4 + 2mn(2n^2 + 3n + 2)}{(1+n)^3(1+mn)} E_1, \tag{5}$$

where m is the modulus ratio E_2/E_1 and n is the thickness ratio h_2/h_1 of the two layers. Here we take layer 1 as PS and layer 2 as P(S-I-S). The thickness ratio at each position can be obtained by measuring the thickness profile of each layer before transferring to the surface of PDMS substrate. Interferometry (Filmetrics, Inc.) was used to measure the film thickness. Figure 6 illustrates the thickness profile of each film and the laminated layer. The thickness profile of the bi-layer was substituted into Eq. (3) to calculate the effective modulus, E_{eff}, of the bi-layer. The two films were then transferred from the silicon wafer to the surface of the pre-stretched PDMS slab. The two films were overlapped so that there were three regions: pure PS, PS-P(S-I-S) bilayer, and pure P(S-I-S). The pure PS and pure P(S-I-S) sections can be used to measure the modulus of PS and P(S-I-S) individually as an internal calibration. The bucking wavelength of both the laminated and individual layers was measured using SALS as described in the previous section. Figure 7 shows the modulus profile of the laminate. The calculated E_{eff} is also shown and the agreement is promising. Using the current technique and materials, the modulus of the laminate exhibited a factor of 3 decrease in modulus from the PS-rich region to the P(S-I-S)-rich region. Equation (5) reveals that E_{eff} is more sensitive to thickness ratio than modulus ratio of the two materials, thus steeper modulus gradients can be made by precisely tuning the thickness ratio between each layer. The entire measurement described here was conducted in less than 10 min, demonstrating that this technique is conducive to high-throughput methodologies and could be applied to other problems where material optimization is paramount.

ACKNOWLEDGMENTS

CMS and CH acknowledge the NIST National Research Council Postdoctoral Fellowship Program.

[1] A. A. Elshabini-Riad and E. D. Barlow, *Thin Film Technology Handbook* (McGraw-Hill, New York, 1997).
[2] H. Namatsu, K. Kurihara, M. Nagase, K. Iwadate, and K. Murase, Appl. Phys. Lett. **66**, 2655 (1995).
[3] H. B. Cao, P. F. Nealey, and W.-D. Domke, J. Vac. Sci. Technol. B **18**, 3303 (2000).
[4] T. Tanaka, M. Morigami, and N. Atoda, Jpn. J. Appl. Phys., Part 1 **32**, 6059 (1993).
[5] M. R. VanLandingham, J. Res. Natl. Inst. Stand. Technol. **108**, 249 (2003).
[6] A. G. Every, Meas. Sci. Technol. **13**, R21 (2002).
[7] D. Du, O. K. C. Tsui, Q. Zhang, and H. He, Langmuir **17**, 3286 (2001).
[8] R. Hartschuh *et al.*, J. Polym. Sci., Part B: Polym. Phys. **42**, 1106 (2004).
[9] J. A. Forrest, K. Dalnoki-Veress, and J. R. Dutcher, Phys. Rev. E **58**, 6109 (1998).
[10] D. Schneider, T. Witke, T. Schwarz, B. Schöneich, and B. Schultrich, Surf. Coat. Technol. **126**, 136 (2000).
[11] M. G. Allen, M. Mehregany, R. T. Howe, and S. D. Senturia, Appl. Phys. Lett. **51**, 241 (1987).
[12] M. K. Small and W. D. Nix, J. Mater. Res. **7**, 1553 (1992).
[13] J. J. Vlassak and W. D. Nix, J. Mater. Res. **7**, 3242 (1992).
[14] D. Maier-Schneider, J. Maibach, and E. Obermeier, J. Microelectromech. Syst. **4**, 238 (1995).
[15] C. M. Stafford *et al.*, Nat. Mater. **3**, 545 (2004).
[16] G. S. Gough, C. F. Elam, and N. A. de Bruyne, J. R. Aeronaut. Soc. **44**, 12 (1940).
[17] M. A. Biot, J. Appl. Mech. **4**, 1 (1937).
[18] H. G. Allen, *Analysis and Design of Structural Sandwich Panels* (Pergamon, New York, 1969)
[19] A. L. Volynskii, S. Bazhenov, O. V. Lebedeva, and N. F. Bakeev, J. Mater. Sci. **35**, 547 (2000).
[20] J. Groenewold, Physica A **298**, 32 (2001).
[21] D. B. Chrisey, A. Pique, J. Fitz-Gerald, R. C. Y. Auyeung, R. A. McGill, H. D. Wu, and M. Duignan, Appl. Surf. Sci. **154-155**, 593 (2000).
[22] Equipment and instruments or materials are identified in the paper in order to adequately specify the experimental details. Such identification does not imply recommendation by NIST, nor does it imply the materials are necessarily the best available for the purpose.
[23] C. Harrison, C. M. Stafford, W. Zhang, and A. Karim, Appl. Phys. Lett. **85**, 4016 (2004).

Downloaded 24 May 2005 to 129.6.154.144. Redistribution subject to AIP license or copyright, see http://rsi.aip.org/rsi/copyright.jsp